Geomechanics and Engineering, *Vol. 30, No. 6 (2022) 579-586*
https://doi.org/10.12989/gae.2022.30.6.579

Evaluation of seismic p-y_p loops of pile-supported structures installed in saturated sand

Jungwon Yun[1a], Jintae Han*[2] and Doyoon Kim[3b]

[1]*Department of Civil Engineering, Korea Army Academy at Yeongcheon, Yeongcheon, Korea*
[2]*Department of Geotechnical Engineering Research, Korea Institute of Civil Engineering and Building Technology, Gyeonggi, Korea*
[3]*Department of Civil Engineering, Korea Army Academy at Yeongcheon, Yeongcheon, Korea*

(*Received June 30, 2022, Revised September 8, 2022, Accepted September 12, 2022*)

Abstract. Pile-supported structures are installed on saturated sloping grounds, where the ground stiffness may decrease due to liquefaction during earthquakes. Thus, it is important to consider saturated sloping ground and pile interactions. In this study, we conduct a centrifuge test of a pile-supported structure, and analyze the p-y_p loops, p-y_p loops provide the correlation between the lateral pile deflection (y_p) and lateral soil resistance (p). In the dry sand model (UV67), the p-y_p loops stiffness increased as ground depth increased, and the p-y_p loops stiffness was larger by approximately three times when the pile moved to the upslope direction, compared with when it moved to the downslope direction. In contrast, no significant difference was observed in the stiffness with the ground depth and pile moving direction in the saturated sand model (SV69). Furthermore, we identify the unstable zone based on the result of the lateral soil resistance (p). In the case of the SV69 model, the maximum depth of the unstable zone is five times larger than that of the dry sand model, and it was found that the saturated sand model was affected significantly by kinematic forces due to slope failure.

Keywords: centrifuge model test; dynamic p-y_p loops; liquefaction; pile-supported structure; unstable zone; unstable zone

1. Introduction

A pile-supported wharves is a structure that supports the top plate with piles. Several instances of slope failure during earthquakes have been reported previously (PIANC 2001). Therefore, it is essential to consider lateral soil-pile interactions in seismic design of piles. Since the lateral soil resistance (p) exhibits a nonlinear relationship with the lateral pile deflection (y_p), a beam on a nonlinear Winkler foundation model (the ground stiffness substitutes for the stiffness of several springs) is commonly applied in geotechnical engineering (Nguyen *et al.* 2018).

Several studies have been conducted to derive the p-y_p curve through static and cyclic tests since the 1970s to simulate the soil and piles interaction (Matlok 1970, Reese *et al.* 1974, Murchinson and O'neill 1984). Since the 1990s, 1 g shaking table tests and dynamic centrifuge tests have been conducted to examine the behavior characteristics of soil and piles subjected to seismic loads using a spring model (Nogami *et al.* 1992, Boulanger *et al.* 1999, Gerolymos and Gazetas 2005, Yoo *et al.* 2013). However, these studies focus only on piles penetrating the horizontal ground.

Recently, the p-y_p curve has been investigated for piles installed on sloped ground. Tran *et al.* (2021a) derived the lateral soil resistance (p) and lateral pile deflection (y_p) through a centrifuge test. They subsequently conducted a 3D numerical analysis of the free-field ground, computed ground deformation (y_s), and relative displacement of ground and piles (y) using the dynamic centrifuge model tests. The characteristics of soil-pile interaction were analyzed with single or group piles, behavior direction, and fixation of piles. Additionally, an application of the suggested p-y_p curve using a pseudo-static analysis was demonstrated.

Nguyen *et al.* (2018) performed centrifuge tests on sloped ground and derived the p-y_p loops of penetrated group piles at the slope. They found an unstable zone on the p-y_p loops and explained that the unstable zone could be changed according to the relative density of the ground. Unstable zone denotes an area that can generate additional kinematic soil force on the pile because the soil flow is faster than the movement of the pile (Nguyen *et al.* 2018). Furthermore, they emphasized that an unstable zone can be applied to predict the horizontal behavior of piles under dynamic loads.

Yun and Han (2021) performed dynamic centrifuge model tests on horizontal and sloped ground, and p-y_p loops were derived from the tests. These derived loops were compared with the existing elastic soil spring model, and the appropriate soil spring model was selected. Then, a response spectrum analysis was performed using the selected spring method, and the applicability of the selected modeling method was evaluated. Yun *et al.* (2022) conducted a numerical analysis using the spring model

*Corresponding author, Ph.D.
E-mail: jimmyhan@kict.re.kr
[a]Assistant Professor
E-mail: 92creative@naver.com
[b]Lecturer
E-mail: kds821821@naver.com

ISSN: 2005-307X (Print), 2092-6219 (Online)

Table 1 Model scaling factors

	Centrifuge Scaling factors		Centrifuge Scaling factors
Acceleration	n^{-1}	Mass	n^3
Velocity	1	Force	n^2
Length	n	Stress	1
Time (dynamic)	n	Pile stiff. (EI)	n^4
Mass density	1	Moment	n^3

Table 2 Prototype and model properties (scale factor=60)

Pile properties	Prototype	Model	Unit
Diameter	914	14	mm
Thickness	14	0.9	mm
Length	18,000	300	mm
Density	78.5	26.4	$kN \cdot m^{-3}$
Flexural rigidity	7.92×10^5	0.061	$kN \cdot m^2$

suggested by Yun and Han (2021) and verified that the spring model appropriately simulates the experimental results.

Thus, the p-y_p loop has been applied to simulate soil-pile interaction, and it has been applied to identify unstable zones on sloping ground. However, the above studies were conducted on dry sand, studies on the p-y_p loop of Pile-supported structures installed in saturated sloping ground considering practical scenarios have not been reported. Investigating this problem is necessary because liquefaction can occur in the saturated sloped ground, deteriorating the ground stiffness. Therefore, this study conducted the centrifuge tests, and p-y_p loops were derived based on the experiment. Next, the possible unstable zone in the sloped ground during an earthquake was derived using the lateral soil resistance (p).

In general, the behaviour of the soil and pile may vary depending on the frequency characteristics of the input motion (Li *et al.* 2016). However, in this study, the effect of different frequency characteristics was not considered, and a seismic motion conforming to Korean design standards (MOF, 2014) was produced and excited.

2. Centrifuge modeling

Centrifuge testing can closely simulate the ground-confining pressure by applying additional centrifugal forces to the model (Haigh and Madabhushi 2010, Lees and Richards 2011, Kim and Choi 2017, Park *et al.* 2021). Table 1 shows the model scaling factors between the prototype and model structure applying in the centrifuge model experiment (McCullough *et al.* 2007). When applying the scaling factors, the prototype scale's behaviour could be expected through model scale test results. Looking at the table, a n-fold difference occurred in the time domain of the prototype and model structure. If an earthquake lasts n seconds in a prototype structure, the earthquake lasts 1/n second in the experimental model of 1/n time scale. By multiplying the experimental model by the scaling factor (n), the time/frequency domain of the prototype structure

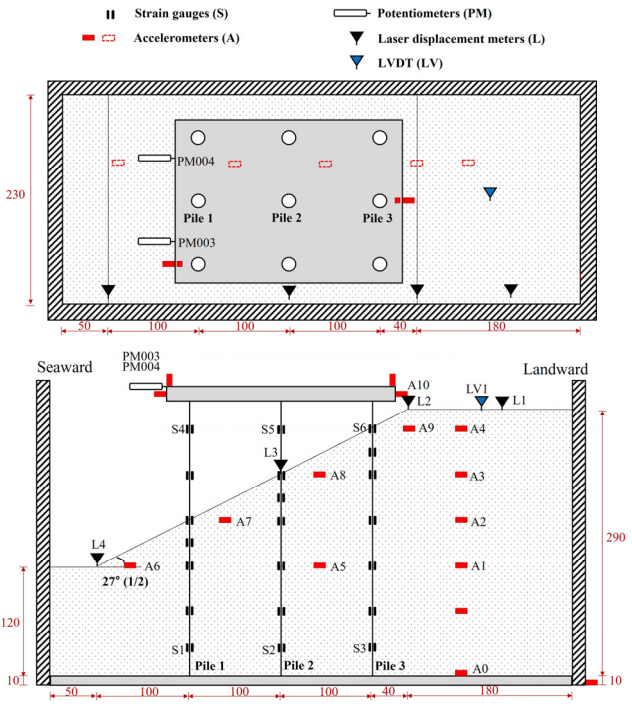

Fig. 1 Schematic diagram of UV67 model (dimension in model scale, unit: mm)

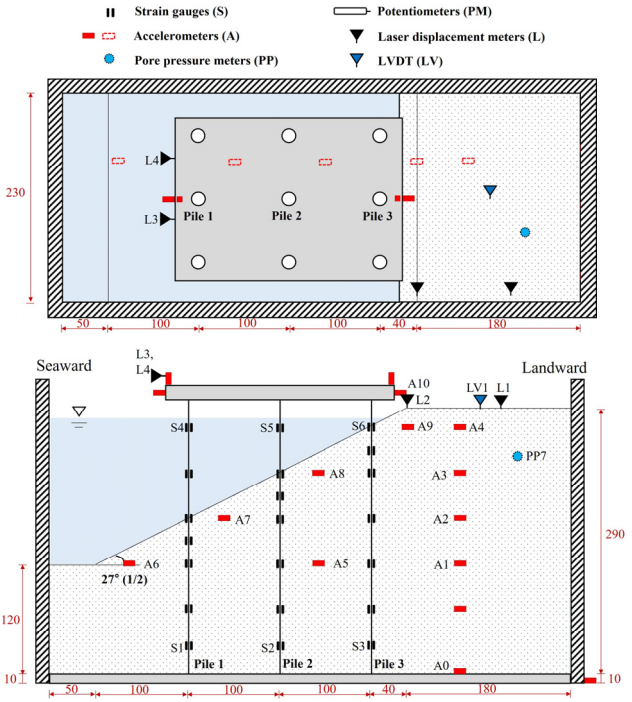

Fig. 2 Schematic diagram of SV69 model (dimension in model scale, unit: mm)

can be expected. According to the Tran *et al.* (2021b) performed the centrifuge model test and 3D dynamic analysis, the dynamic time domain between the test and analysis seems to match.

In this study, a centrifugal model tester was used cooperatively with the Korea Advanced Institute of Science and Technology (KAIST). The device, which has a rotation

Table 3 silica sand properties

Soil properties	Silica sand	Unit
Unified soil classification system	SP	-
Coefficient of curvature	1.16	-
Coefficient of uniformity	1.96	-
Specific gravity of soil	2.63	-
Maximum dry unit weight	16.5	$kN \cdot m^{-3}$
Minimum dry unit weight	12.4	$kN \cdot m^{-3}$

Table 4 Test program

Model	Seismic motion	Input acceleration amplitude (bedrock motion, g)
UV67 model	Artificial	0.01, 0.08, 0.11, 0.15, 0.2, 0.24, 0.27
SV69 model	Artificial	0.02, 0.08, 0.16, 0.26

diameter of 5 m, can be implemented under a maximum load of 240 g-ton (Kim *et al.* 2013, Yun *et al.* 2019, Yun and Han 2020). All tests in this study were performed under a centrifuge acceleration of 60 g, the similarity law of the centrifuge model is listed in Table 2, considering the flexural stiffness of the pile (McCoullough *et al.* 2007).

Figs. 1 and 2 show the overall layout of the model, including the soil layer, structural model, and measuring device. The experimental setup included displacement meters, accelerometers, strain gauges, and pore water pressure transducer to measure the displacement and acceleration of the ground and structures, pile moment, and excess of pore water pressure. In the model, UV and SV represent unsaturated soil/vertical piles and saturated soil/vertical piles, respectively, and 67 and 69 indicate the relative ground densities (%). First, in the case of the UV67 model, laser displacement meters and a LVDT were installed to measure the settlement of the slope. On the other hand, in the case of the SV69 model, it is difficult to apply the above instruments to the part filled with water, so a grid pattern film was attached to the side of the soil box to capture the soil displacement with high-speed camera (1200 samples/sec). For the experimental model, a section of a Pile-supported structure in Pohang, South Korea was selected. The experimental models comprised nine piles in a wharf segment, arranged in three rows and three columns. In this experiment, strain gauges were attached only to the piles in row 2, and the piles in each column in low 2 were named Pile 1, Pile 2, and Pile 3, respectively. silica sand was used for ground modeling (Table 3). Further details on the structure installation, ground and slope status, and ground saturation are provided by Yun *et al.* (2021). In the study of Yun *et al.* (2021), the response spectrum analysis was performed base on the experimental results to evaluate the seismic performance of the pile-supported structure installed in the saturated sandy soil. In this study, based on the experimental results of Yun *et al.* (2021), we evaluated the dynamic p-y_p loops and focused on identifying the unstable zone.

Artificial seismic motion was used in accordance with 'Standards and commentary on the design of ports and fishing ports' established by the Ministry of Oceans and Fishery in Korea, as shown in Fig. 3(a) (MOF 2014). In the

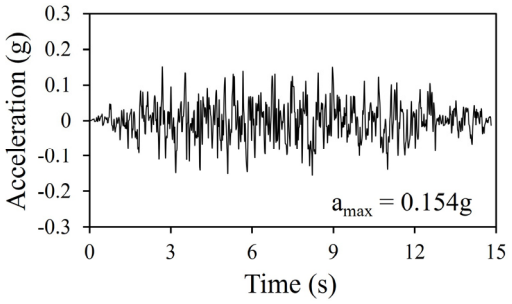

(a) Input motion (artificial wave)

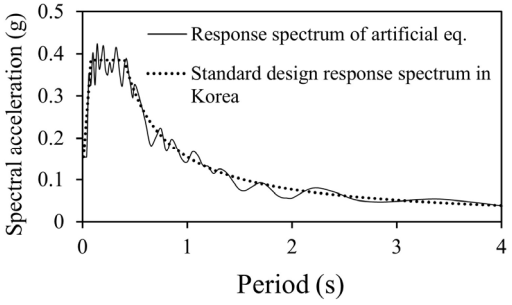

(b) response spectrum curve

Fig. 3 Input motion and response spectrum

case of the ground acceleration used for seismic design, it can be represented as a response spectrum curve. The damping ratio was generally 5%. Fig. 3(b) shows that the response spectrum curve of the input seismic motion and its standard design response spectrum curve matched well. The maximum amplitudes of the input seismic waves are listed in Table 4. As a dry ground model, the UV67 model used seven different bedrock accelerations. In contrast, the SV69 saturated ground model selects four different bedrock accelerations, owing to the minimization of the ground disturbance caused by liquefaction.

3. Dynamic centrifuge model test results

3.1 Result of ground subsidence

Fig. 4 shows the ground subsidence caused by spinning and vibration in the UV67 and SV69 models (in prototype scale). Spinning is the process of increasing the centrifugal acceleration of the experimental model to the g level, corresponding to a similar ratio (n). During spinning, ground subsidence can occur due to variations in ground stress, even when the centrifugal force increases slightly. The UV67 model shows maximum subsidence of 176 mm after spinning and final subsidence of 440 mm after seven seismic inputs (prototype). Moreover, the SV69 model had maximum subsidence of 960 mm and final subsidence of 1066 mm after four seismic inputs. The location where the maximum subsidence occurred is the crest of the top slope, and the edge of the slope indicate the upslope part. This experimental model calculates the relative density of the ground considering spinning, such that the density in the saturated ground increases by 6%, from 63% to 69%.

In the ground subsidence result shown in Fig. 4(b), there

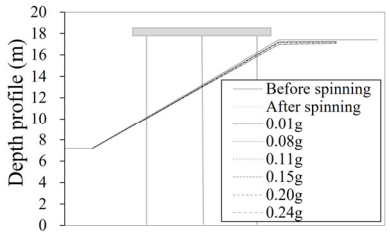

(a) UV67 model

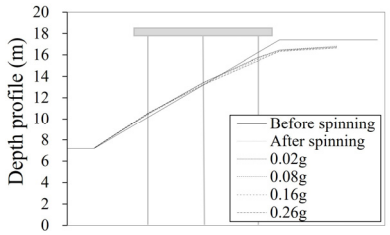

(b) SV69 model

Fig. 4 Ground settlement of model during spinning and shaking

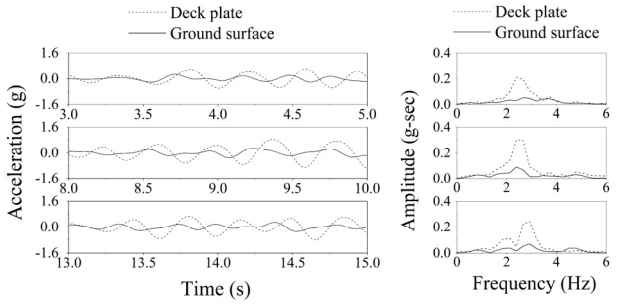

(a) UV67 model (input acceleration : 0.27g)

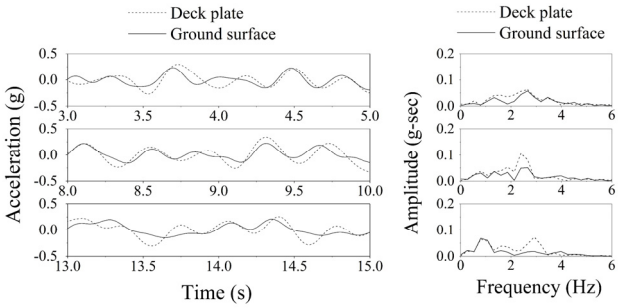

(b) SV69 model (input acceleration: 0.26 g)

Fig. 5 Phase analysis and FFT (Fast Fourier Transform) curve between the ground surface (A2) and deck plate (A3) (in prototype scale)

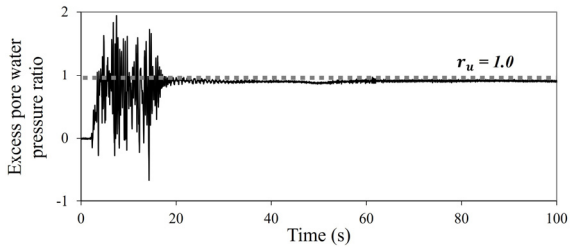

Fig. 6 Excess pore water pressure ratio of PP7 (SV69 model, input acceleration: 0.26 g, in prototype scale)

was a planar failure at the top of the slope. The surface of this failure crosses the edge of the slope, it was found on the ground with a fractured zone and weakness layer (Ling *et al.* 1999). This graph shows that slope failure occurred only at the top of the slope. It is interpreted that piles installed on the slop acts as stabilized piles, and constrain failure in the middle of the slope.

3.2 Acceleration phase difference

Fig. 5(a) shows the acceleration phase and frequency response analysis results of the UV67 model (input bedrock acceleration of 0.27 g). The acceleration response is classified into three different time zones: beginning (3~5 s), middle (8~10 s), and end (13~15 s). The highest response is shown in the 2.5~3 Hz frequency area, and the response at the deck plate is higher than that on the ground surface. As a result of the comparison between the acceleration phase at the deck plate and that on the ground surface, the force of inertia at the deck plate does not match the kinematic force phase on the ground surface. Since the inertia force on the piles pushes the ground, the piles are supported by the adjacent ground, resulting in a phase difference in the dry ground model.

The acceleration phase and frequency response results for the SV69 model are shown in Fig. 5(b). The highest response was observed in the frequency range of 2.5 to 3 Hz, with no significant difference in response amplitudes between the deck plate and ground surface. Moreover, the force of inertia at the deck plate was similar to the kinematic force on the ground surface, caused by liquefaction in saturated ground followed by earthquakes. This is because when liquefaction occurred, the soil flow of the slope produces an additional kinematic force that pushes the pile, and the soil and pile appear to move together.

The excess pore water pressure ratio (r_u) is generally calculated to determine the liquefaction in experimental models. r_u can be calculated by dividing the excess pore pressure at a certain depth by initial vertical effective stress at that depth. It is judged that liquefaction occurs when r_u is close to 1 (Manandhar *et al.* 2020). In Figure 6, the r_u on the ground surface was approximately 1 over 100 s, implying that liquefaction occurred at the saturated ground surface.

4. Dynamic p-y_p loops

4.1 The calculation of dynamic p-y_p loops

The soil-pile interaction under lateral loads can generally be represented by the relationship between the lateral pile deflection (y_p) and lateral soil resistance (p). Here, the nonlinear p-y_p loop is calculated from the experimental results.

First, the moments of piles by depth were calculated by multiplying the bending stiffness of piles by the measured strain data (Yoo *et al.* 2013). Next, the lateral soil resistance (p) and lateral pile deflection (y_p) were calculated by

differentiating or integrating the moment of piles by depth according to Eqs. (1) and (2), as shown below. MATLAB was used to develop the p-y_p loop (MATLAB, 2016). In the equations, M(z) is the moment of the piles with the depth measured experimentally, EI is the bending stiffness of the piles, and z is the depth from the ground.

$$p = \frac{d^2}{dz^2} M(z) \tag{1}$$

$$y_p = \iint \frac{M(Z)}{EI} dz \tag{2}$$

When measuring the strain from the shaking table, electrical signals can induce data noise that needs to be removed. In addition, the strain must be transformed into the curve equation because it is the response calculated from the specific depth. Yun and Han (2021) addressed the data processing method to solve this problem.

Figs. 7 and 8 show the p-y_p loops of the UV67 and SV69 models, respectively. The UV67 model results show that the response of the 0.27 g of input bedrock acceleration is applied to the base. The SV69 model result shows that the response of 0.26 g of input bedrock acceleration is applied to the base. In each graph, the responses depending on three different depths from the ground surface, 0.5D, 1.5D, and 3.0D (D: diameter of pile) represent 1-cycle loops where the amplitude of the p-y loops is the highest.

The stiffness of the p-y_p loop in the figures can be calculated from the inclination from the center of the x and y axes to the peak point of the loop. First, the stiffness of the p-y_p loop and the depth of the ground exhibit a positive relationship, as shown in Fig. 7, in the dry sand model. As the depth of the ground increases, the lateral soil resistance (p) increases, but the lateral pile deflection (y_p) decreases because the confining pressure of the ground increases as the ground deepens. In addition, when the pile moved upslope, the inclination of the p-y_p loop was approximately three times higher than that when the pile moved downslope, indicating that the gap in the earth pressure between the upslope and downslope directions significantly influences the inclination of the p-y_p loop. Specifically, massive lateral soil resistance is caused by passive earth pressure when a pile moves in the upslope direction. Secondly, as shown in Fig. 8, in the saturated sand model, pile 1 shows an increase in the stiffness of the p-y_p loop as the depth of the ground increases. However, the closer the location of the pile to the top crest of the slope (toward pile 3), the less significant the gap in the stiffness of the p-y_p loop depending on the depth of the ground. Furthermore, the slope of the p-y_p loops at pile 1 was larger when the pile moved in the upslope direction than when it moved in the downslope direction. However, there was no significant difference in the slope of the p-y_p loop according to the direction as the pile moved to pile 3, possibly attributed to the fact that liquefaction on the ground surface results in a significant reduction in the ground stiffness. During liquefaction, the lateral soil resistance (p) was approximately zero, and the passive earth pressure had no significant impact on the resistance based on the ground slope.

Fig. 9 shows the p-y_p loop of pile 3, depending on the time when the stiffness is the highest. Fig. 9(a) shows the results of the dry sand model, which indicate that the stiffness of the p-y_p loop when a pile moves in the upslope direction is larger than when a pile moves in the downslope direction. However, there was no significant difference in the stiffness over time. In the other hand, the saturated ground, as seen Fig. 9(b), the lateral soil resistance (p) is

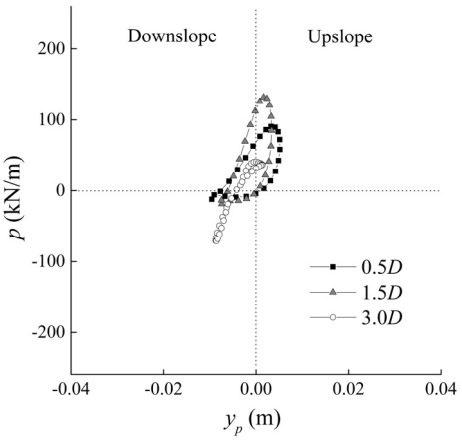

(a) Pile 1

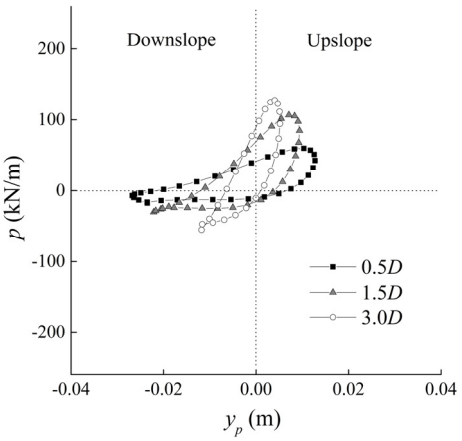

(b) Pile 2

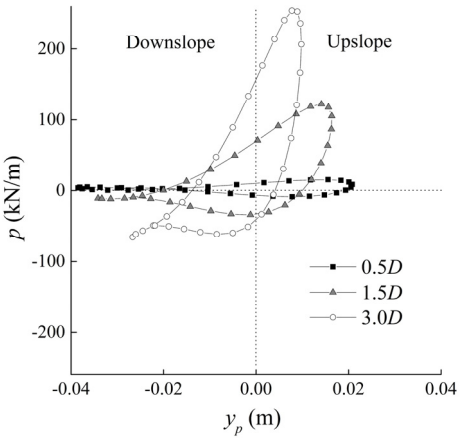

(c) Pile 3

Fig. 7 Dynamic p-y_p loops at various depth (UV67 model, input bedrock acceleration=0.27g)

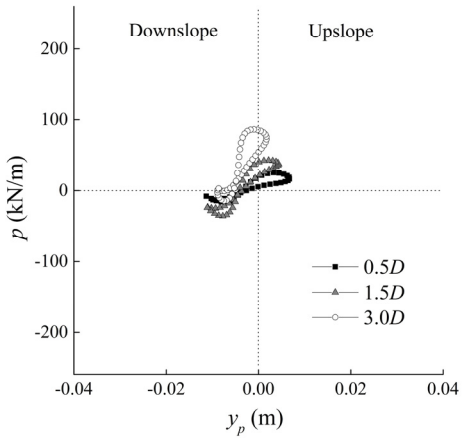

(a) Pile 1

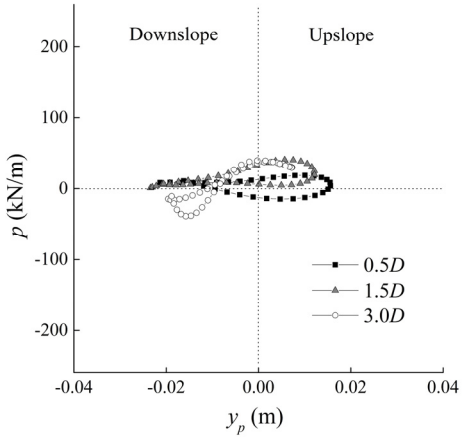

(b) Pile 2

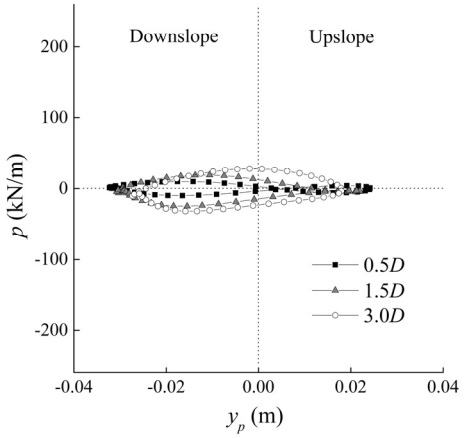

(c) Pile 3

Fig. 8 Dynamic p-y_p loops at various depth (SV67 model, input bedrock acceleration=0.26 g)

close to 0 near 10 s, but it shifts to a positive value in the second quadrant over time. It is assumed that an additional kinematic force is applied by the ground slope pushing the pile because the soil flow is faster than that of the pile movement. Moreover, the lateral pile deflection (y_p) gradually increases in the negative direction over time. It is thought that the pile gradually moves in the seaward

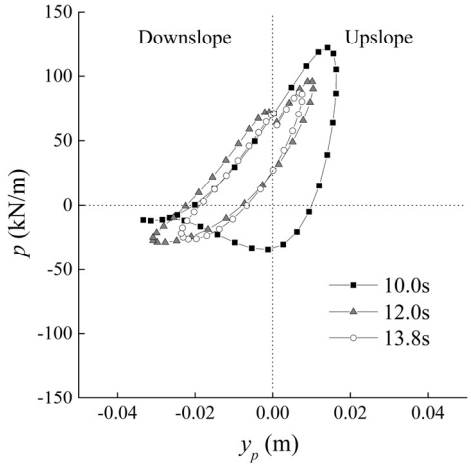

(a) UV67 model (input bedrock acceleration: 0.27 g)

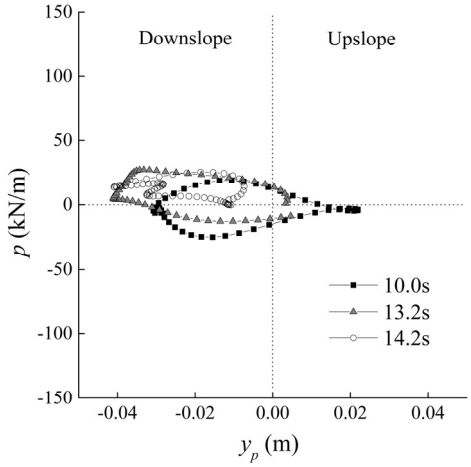

(b) SV69 model (input bedrock acceleration: 0.26 g)

Fig. 9 Dynamic p-y_p loops according to the time (1.5D depth, Pile 3)

direction due to the kinematic force of the slope. This result implies the importance of the kinematic force of the ground on the sloped ground. Therefore, it is necessary to develop a seismic design method that considers the kinematic force of the ground.

4.2 The soil-pile interaction by unstable zone

As described above, when the liquefaction occurred, the soil flow of the slope is faster than that of the pile movement, and an additional kinematic force is applied to the pile, resulting in the maximum values in the second quadrant of the p-y_p loops. Nguyen *et al.* (2018) defined an area where the maximum value of p-y_p loops occurred in the second quadrant as an unstable zone and derived the unstable zone of piles penetrating the dry sand ground.

In this study, the lateral soil resistance (p) according to the ground saturation and the direction of pile movement was calculated to evaluate the interaction between the sloped ground and pile, thereby obtaining the unstable zone. Figs. 10 and 11 show the lateral soil resistance and unstable zone of the UV67 model (input bedrock acceleration: 0.27

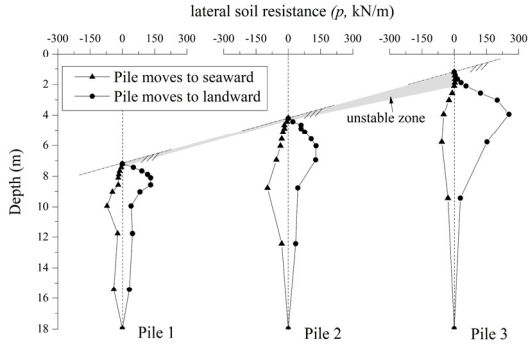

Fig. 10 Max. lateral soil resistance (p) distribution curves of UV67 model (input bedrock acc.: 0.27 g)

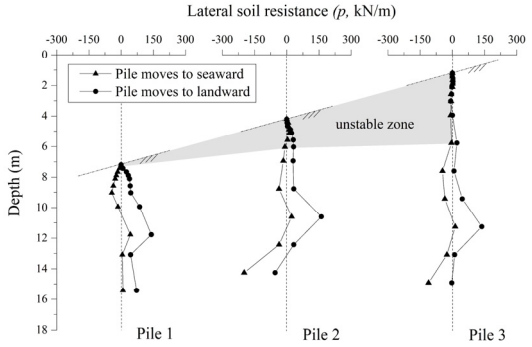

Fig. 11 Max. lateral soil resistance (p) distribution curves of SV69 model (input bedrock acc.: 0.26 g)

g) and SV69 model (input bedrock acceleration: 0.26 g) according to the behavioral direction, respectively.

First, in the case of the dry sand model shown in Figure 10, the depth at which the lateral soil resistance (p) is maximized fluctuates according to the behavior direction. For example, as a pile moves landward (upslope direction), the depths at which the maximum lateral soil resistance occurs at piles 1, 2, and 3 are approximately 1 D, 2 D, and 3 D, respectively. In the other hand, the depths of the piles are approximately 3 D, 5 D, and 5 D, while the pile moves seaward (downslope direction). These results also show that the latter values are deeper than the former because the gap of passive earth pressure on the slope differs according to the behavioral direction of the pile. Comparing the maximum lateral soil resistance (p), a pile moving in the landward is 4.4 times higher than that in the seaward at pile 3, 1.85 times higher than at pile 1. It is thought that pile 3 is the head pile under the largest passive earth pressure.

Second, there was not much difference in the lateral soil resistance (p) of the slope according to the behavior direction on the saturated soil, as seen in Fig. 11. In addition, it is exceedingly small up to a depth of approximately 7 m because the passive earth pressure declines due to the liquefaction at the top of the slope in the model. However, an unstable zone was observed at the depth of the slope. It is thought that liquefaction causes the kinematic force of the slope such that the movement of the ground becomes faster compared to that of the piles, following the maximum value of the p-y_p loops in the second quadrant.

Comparing the dry sand model to the saturated sand model, the depths corresponding to the unstable zone at piles 1, 2, and 3 were 0.25 D, 0.25 D, and 1.0 D in the dry sand model, and 0.25 D, 2.0 D, and 5.0 D in the saturated sand model, signifying a five-fold difference between them. Consequently, it appears that the influence of the slope kinematic force on the saturated sloping ground was remarkably higher than that on the dry sloping ground.

This study focuses on an unstable zone and can be implemented to simulate the soil-pile interaction under dynamic loads on sloped ground. As an unstable zone can occur in a deeper position in the saturated sloped ground, the concept of the unstable zone should be examined for applicability to practical areas.

5. Conclusions

In this study, the p-y_p loops were calculated based on the experiment to identify potential unstable zones on the sloped ground during earthquakes. The main conclusions of this study are as follows.

- Planar failure occurred at the top of the slope due to the subsidence of the saturated ground. The piles on the slope served as stabilized piles, constraining the failure at the middle of the slope.
- In terms of the acceleration phase, the kinematic force of the ground and the inertia force of the deck plate of the dry sand model were out of phase, whereas they were in phase in the saturated ground model. In the saturated sand model, additional kinematic forces are generated in the ground as the soil flow occurs due to liquefaction. Consequently, it causes the ground to push the piles, thereby creating a concurrent movement of the ground and piles.
- The p-y_p loops of the dry sand model indicate that the stiffness of the p-y_p loops gradually increases as the ground becomes deeper, it is three times larger when a pile moves in the upslope direction than when it moves in the downslope direction. Considering saturated sand, no significant difference was noted depending on the depth of the ground and the direction of pile movement, caused by liquefaction deteriorating the ground stiffness.
- The lateral soil resistance (p) was calculated to evaluate the soil-pile interaction. An unstable zone was also obtained, which is the maximum value in the second quadrant of the p-y_p loops. In case of the saturated sand model, the unstable zone was five times larger than that of the dry sand model, indicating that saturated sand is more influenced by the kinematic force caused by slope failure.
- In this study, the p-y_p loops were calculated based on the experiment, and identify the unstable zones on the sloped ground during earthquake. However, since the soil displacement (y_s) was not considered in this study, the relative displacement between the saturated sloping ground and piles (y) could not be derived. In the future, studies on p-y curves are required to properly analyze the dynamic interaction between the saturated sloping ground and piles.

Acknowledgments

This research was supported by the "Korea Institute of Civil Engineering and Building Technology (KICT), grant number 20220332-001" and "Korea Institute of Marine Science & Technology Promotion (KIMST), grant number 2016-0065".

References

Boulanger, R.W., Curras, C.J., Kutter, B.L., Wilson, D.W. and Abghari, A. (1999), "Seismic soil-pile-structure interaction experiments and analyses", *J. Geotech. Geoenviron. Eng.*, **125**(9), 750-759. https://doi.org/10.1061/(ASCE)1090-0241(1999)125:9(750).

Gerolymos, N. and Gazetas, G. (2005), "Phenomenological model applied to inelastic response of soil-pile interaction systems", *Soil. Found.*, **45**(4), 119-132. https://doi.org/10.3208/sandf.45.4_119.

Haigh, S.K. and Gopal Madabhushi, S.P. (2011), "Centrifuge modelling of pile-soil interaction in liquefiable slopes", *Geomech. Eng.*, **3**(1), 1-16. https://doi.org/10.12989/gae.2011.3.1.001.

Kim, D.S., Kim, N.R., Choo, Y.W. and Cho, G.C. (2013), "A newly developed state-of-the-art geotechnical centrifuge in Korea", *KSCE J. Civil Eng.*, **17**(1), 77-84. https://doi.org/10.1007/s12205-013-1350-5.

Kim, Y.S. and Choi, J.I. (2017), "Nonlinear numerical analyses of a pile-soil system under sinusoidal bedrock loadings verifying centrifuge model test results", *Geomech. Eng.*, **12**(2), 239-255. https://doi.org/10.12989/gae.2017.12.2.239.

Lees, A.S. and Richards, D.J. (2011), "Centrifuge modelling of temporary roadway systems subject to rolling type loading", *Geomech. Eng.*, **3**(1), 45-59. https://doi.org/10.12989/gae.2011.3.1.045.

Li, Z., Escoffier, S. and Kotronis, P. (2016), "Centrifuge modeling of batter pile foundations under sinusoidal dynamic excitation", *Bull. Earthq. Eng.*, **14**(3), 673-697. https://doi.org/10.1007/s10518-015-9859-2.

Ling, H.I., Mohri, Y. and Kawabata, T. (1999), "Seismic analysis of sliding wedge: Extended Francais–Culmann's analysis", *Soil Dyn. Earthq. Eng.*, **18**(5), 387-393. https://doi.org/10.1016/S0267-7261(99)00005-6.

Manandhar, S., Kim, S.N., Ha, J.G., Ko, K.W., Lee, M.G. and Kim, D.S. (2021). "Liquefaction evaluation using frequency characteristics of acceleration records in KAIST centrifuge tests for LEAP", *Soil Dyn. Earthq. Eng.*, **140**, 106332. https://doi.org/10.1016/j.soildyn.2020.106332.

MATLAB (2016), MATLAB Version R2016a, a Computer Program, The Mathworks Inc., Natick, MA-USA.

Matlock, H. (1970), "Correlations for design of laterally loaded piles in soft clay", *Proceedings: Second Offshore Technology Conference*, Huston, Texas, USA, April.

McCullough, N.J., Dickenson, S.E., Schlechter, S.M. and Boland, J.C. (2007), "Centrifuge seismic modeling of Pile-supported wharves", *Geotech. Test. J.*, **30**(5), 349-359. https://doi.org/10.1520/GTJ14066.

MOF (Ministry of Oceans and Fisheries) (2014), Design Standards of Harbour and Port, Ministry of Oceans and Fisheries, Sejong, Korea. (in Korean)

Murchison, J.M. and O'Neill, M.W. (1984,), "Evaluation of P-Y relationships in cohesionless soils", *Analysis and Design of Pile Foundations*, 174-191, October.

Nguyen, B.N., Tran, N.X., Han, J.T. and Kim, S.R. (2018), "Evaluation of the dynamic p–yp loops of pile-supported structures on sloping ground", *Bull. Earthq. Eng.*, **16**(12), 5821-5842. https://doi.org/10.1007/s10518-018-0428-3.

Nogami, T., Otani, J., Konagai, K. and Chen, H.L. (1992), "Nonlinear soil-pile interaction model for dynamic lateral motion", *J. Geotech. Eng.*, **118**(1), 89-106.

Park, S., Kim, J.H., Kim, S.J., Park, J.H., Kwak, K.S. and Kim, D.S. (2021), "Centrifuge modelling of rock-socketed drilled shafts under uplift load", *Geomech. Eng.*, **24**(5), 431-441. https://doi.org/10.12989/gae.2021.24.5.431.

PIANC (International Navigation Association) (2001), Seismic Design Guidelines for Port Structures, International Navigation Association, Rotterdam, Netherlands.

Reese, L.C., Cox, W.R. and Koop, F.D. (1974), "Analysis of laterally loaded piles in sand", *Proceeding: 6th Offshore Technology Conference*, Huston, Texas, May.

Tran, N.X., Bong, T., Yoo, B.S. and Kim, S.R. (2021b), "Evaluation of the soil-pile interface properties in the lateral direction for seismic analysis in sand", *Soil Dyn. Earthq. Eng.*, **140**, 106473. https://doi.org/10.1016/j.soildyn.2020.106473.

Tran, N.X., Nguyen, B.N., Yoo, B.S. and Kim, S.R. (2021a), "Slope effect on dynamic p–y backbone curve in dry sand", *Soil Dyn. Earthq. Eng.*, **144**, 106693. https://doi.org/10.1016/j.soildyn.2021.106693.

Yoo, M.T., Choi, J.I., Han, J.T. and Kim, M.M. (2013), "Dynamic P-Y curves for dry sand from centrifuge tests", *J. Earthq. Eng.*, **17**(7), 1082-1102. https://doi.org/10.1080/13632469.2013.801377.

Yun, J.W. and Han, J.T. (2020), "dynamic behavior of pile-supported structures with batter piles according to the ground slope through centrifuge model tests", *Appl. Sci.*, **10**(16), 5600. https://doi.org/10.3390/app10165600.

Yun, J.W. and Han, J.T. (2021), "Evaluation of soil spring methods for response spectrum analysis of pile-supported structures via dynamic centrifuge tests", *Soil Dyn. Earthq. Eng.*, **141**, 106537. https://doi.org/10.1016/j.soildyn.2020.106537.

Yun, J.W., Han, J.T. and Kim, J.K. (2021), "Evaluation of seismic performance of Pile-supported wharves installed in saturated sand through response spectrum analysis and dynamic centrifuge model test", *J. Korean Geotech. Soc.*, **37**(12), 71-87. (in Korean) https://doi.org/10.7843/kgs.2021.37.12.73.

Yun, J.W., Han, J.T. and Kim, S.R. (2019), "Evaluation of virtual fixed points in the response spectrum analysis of a Pile-supported wharf", *Géotechnique Lett.*, **9**(3), 238-244. https://doi.org/10.1680/jgele.19.00013.

Yun, J.W., Jin, T.H. and Kim, J.K. (2022), "Evaluation of the virtual fixed-point method for seismic design of pile-supported structures" *KSCE J. Civil Eng.*, **26**, 596-605. https://doi.org/10.1007/s12205-021-0422-1.

IC